Desalination and Water Treatment
www.deswater.com
doi: 10.5004/dwt.2022.28860

273 (2022) 43–54
October

Parametric investigation of a vacuum membrane distillation system driven by mechanical vapor recompression

Jiaqiang Li[a], Zetian Si[b,*], Yuan Yang[c,*]

[a]*School of Mechanical and Electric Engineering, Soochow University, Suzhou 215021, China*
[b]*College of Mechanical and Electrical Engineering, Wenzhou University, Wenzhou, Zhejiang 325035, China, email: tian3221623@163.com*
[c]*SINOMACH Intelligent (Suzhou) Co., Ltd., Suzhou 215134, China*

Received 23 March 2022; Accepted 18 August 2022

ABSTRACT

This paper focused on employing a vacuum membrane distillation system (VMD) driven by mechanical vapor recompression to achieve the sulfuric acid waste recovery. After establishing the mathematical models with the thermodynamic first and second laws considered simultaneously, the effects of critical parameters on the mass and heat transfer processes were first investigated. Furthermore, the effects of membrane area on thermodynamic characteristic of the system were explored. The simulation results showed that decreasing feed concentration or increasing feed temperature, feed velocity and permeate side pressure could strengthen heat and mass transfer process. Furthermore, increasing membrane area caused the total power consumption to exhibit a decline first followed by a rise and the exergy efficiency to exhibit a first rise followed by a decline. There was an optimal membrane area of 60 m^2 that minimized the total power to 10.04 kW and maximized the exergy efficiency to 19.06% at a feed concentration of 5%, feed temperature of 358.15 K, feed velocity of 1.0 $m \cdot s^{-1}$ and evaporation rate of 200 $kg \cdot h^{-1}$. The research results provide reference and technical support for the treatment of industrial waste acid.

Keywords: Sulfuric acid waste; Vacuum membrane distillation; Mechanical vapor recompression; Heat and mass transfer; Membrane area

1. Introduction

As known as the "mother of the chemical industry", sulfuric acid is widely used in the chemical industry, iron and steel, chlor-alkali, titanium dioxide, nonferrous metals, papermaking and other industries. However, due to the simple production equipment, backward technical conditions and nonstandard operation, the utilization efficiency of sulfuric acid is extremely low, resulting in the production of a large amount of sulfuric acid waste. Direct discharge not only wastes resources, but also pollutes the environment [1–3]. Therefore, recycling such sulfuric acid waste is of great significance.

As a new non-isothermal thermally driven separation technology, vacuum membrane distillation (VMD) separates the solute and solvent in the feed solution under a vacuum environment with the vapor pressure difference on both sides of the hydrophobic membrane as the driving force, so as to realize the concentration and recovery of the feed solution [4]. Due to the hydrophobic microporous membrane as a barrier, VMD has many advantages of high separation efficiency, strong corrosion resistance and mild operating conditions, and VMD can be used in the fields of wastewater treatment, seawater desalination and ultra pure water preparation [5]. In recent years, VMD has become the research hotspot all around the world, and many scholars have done a lot of related researches. Boutikos et al. [6] presented a mathematical model based on the mass and energy balances that would provide useful guide lines for the optimal design

* Corresponding authors.

1944-3994/1944-3986 © 2022 Desalination Publications. All rights reserved.

of a vacuum multi-effect membrane distillation system. Mohamed et al. [7] conducted an experimental study on a vacuum multi-effect membrane distillation system, and concluded that a distillate production can reach 50 $L{\cdot}h^{-1}$ while the temperature of inlet heating water was 353.15 K and the gained output ratio (GOR) varied between 1–1.2. However, it is found that the existing VMD technology has low membrane flux and thermal efficiency, and a large amount of latent heat of vapor has not been recovered and utilized, resulting in a large amount of wasted energy [8].

Mechanical vapor recompression (MVR) is a new type of energy saving and environmental protection technology based on the self-heat recuperation theory [9,10], which effectively uses the latent heat of the secondary vapor compressed by the compressor to heat the feed solution, so it has a high thermodynamic efficiency and produces a high quality distillate with zero-emissions [11,12]. To date, MVR has been widely used in the wastewater treatment, solid drying, seawater desalination and traditional Chinese medicine concentration and other industrial fields [13,14]. Zhou et al. [15] simulated a MVR wastewater treatment system, the results showed that the specific heating energy consumption (SHEC), which was defined as the electric energy consumed by evaporating 1 ton of water, could reach 55.6 $kWh{\cdot}t^{-1}$. Nafey et al. [16] performed comprehensive economic analysis of a multi-effect MVR process for desalination application, the results showed that the multi-effect MVR system had a prominent energy saving performance. However, the existing MVR systems generally has the disadvantages of low separation efficiency and weak corrosion resistance, so it is still difficult to separate sulfuric acid solution with high purity. Therefore, recycling sulfuric acid waste by VMD coupled with MVR will be the development trend in the future.

At present, many researchers have carried out the preliminary research and exploration on the VMD coupled with MVR to concentrate and recover the industrial sulfuric acid waste [17–19]. Li et al. [20] proposed to use the MVR process to recover the latent heat of vapor produced in the VMD process of bioethanol, and predicted that the evaporation energy consumption would be effectively reduced through theoretical analysis, but failed to verify its actual energy saving effect through experiments. Si et al. [21–25] proposed to use MVR coupled with VMD to deal with industrial sulfuric acid waste. Based on the conservation laws of mass and energy, theoretical models of coupling process were established, and the corresponding experimental device was built. The results showed that the latent heat of vapor in the VMD process was effectively recovered by MVR, and the energy consumption of evaporation was significantly reduced. The separation efficiency was 99%, and the SHEC was 145.4 $kWh{\cdot}t^{-1}$, energy saving rate was calculated to be 72.87% compared with the conventional VMD system.

In summary, the research on the concentration and treatment of sulfuric acid solution by MVR coupled with VMD mainly focuses on the separation characteristics and thermodynamic characteristics, and the heat and mass transfer model of the system is initially established. However, the relevant research gap about the coupled system were also evident: (1) The established heat and mass transfer model is not perfect, and the parameters of system components are not matched reasonably, it is difficult to achieve efficient operation for the current MVR coupled with VMD system. (2) The effects of membrane area on system performance were seldom involved about the coupled system in the previous investigations. In this paper, a VMD system driven by the MVR is still selected as the research object, the mathematical models are established with the sulfuric acid solution as feeding, the mass and heat transfer mechanism of sulfuric acid solution in the coupled process of MVR and VMD is further explored. The influences from the operating parameters, such as feed concentration, feed temperature, feed velocity and permeate side pressure on the heat transfer coefficient and mass transfer coefficient are investigated. Furthermore, the effects of membrane area on the compressor power, feed power, total power and exergy efficiency are also studied, and the optimal membrane area to achieve the highest exergy efficiency is also achieved. The research method and relevant obtained results provide significant references for the implementation and further optimization of the current system.

2. Experiment

2.1. System description

The system schematic diagram is presented in Fig. 1. The system mainly includes feed tank, VMD module, compressor, heat exchanger, distilling tank, vacuum pump, and other auxiliary equipment. The VMD module contains many hollow fibers with polytetrafluoroethylene material. Taking the sulfuric acid solution as the feed solution, the feed solution is first preheated to a certain temperature by an external heat source, then the preheated solution is pumped to the shell side of the VMD module by a feed pump, while the tube side of VMD module forms a vacuum environment under the action of a vacuum pump. The feed

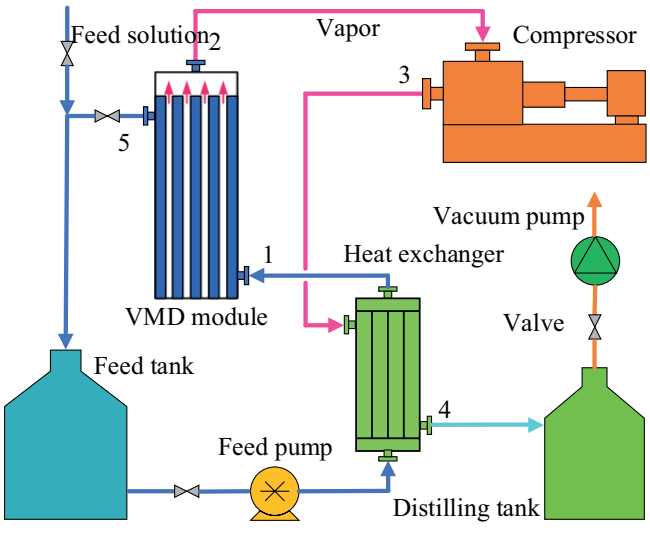

Fig. 1. Flow diagram of the current system.

solution will be separated into the concentrated solution and vapor through the membrane with the help of driving pressure difference across the membrane. The produced vapor flows out of the tube side and enters the compressor to compress, to increase its saturation temperature and pressure, while the concentrated solution goes back to the feed tank to concentrate continuously. The higher temperature vapor will enter the heat exchanger to heat the feed solution by releasing the heat, then condense into the liquid water and finally be collected into the distilling tank. The whole evaporation process of feed solution is carried out under the vacuum conditions utilizing the internal vapor latent heat.

2.2. Experiment material and method

In order to verify the established mathematical models, an experimental device of the coupled system was built, as shown in Fig. 2. The feed tank was made of CPVC material; The VMD module was produced by Nanjing Langtian Technology Co., LTD. with a porosity of 80% and a membrane area of 20 m^2. However, the shell of the VMD module was made of CPVC material with corrosion resistance; The feed pump adopted the acid-proof fluorinated plastic magnetic pump produced by Anhui Jiangnan Pump and Valve Group Co., Ltd., the brand, power and rated flow rate were CQB65-50-125F, 4 kW and 25 $m^3 \cdot h^{-1}$; The heat exchanger was made of acid resistant material with the heat exchanging area of 4 m^2. All other pipes and valves were made of CPVC pipes. In addition, the measuring system needed to be reformed to improve the anti-corrosion performance, focusing on the flow meter and temperature meter. The flow meter was equipped with polytetrafluoromaterial, and the thermometer was employed as PT100 temperature sensor with digital display, and its measuring probe was equipped with polytetrafluoromaterial of a certain thickness, with a measuring range of 273.15–373.15 K. The pressure gauge was selected as vacuum gauge with a brand of YZ-100 and a range of –0.1–0 MPa. Since the experimental device was built in Nanjing Langtian Technology Co., LTD., the feed solution was directly from the dilute sulfuric acid solution (2%–10%) used in the enterprise field production.

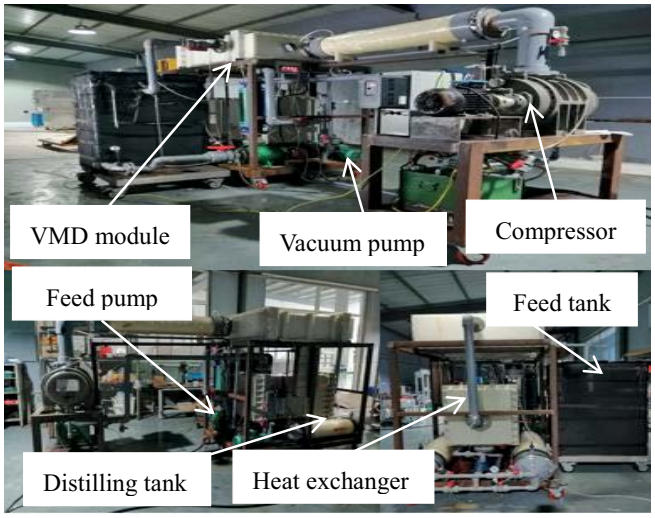

Fig. 2. Photo of the experimental system.

3. Theory

To simulate and obtain the relevant characteristics of the current system, the mathematical models are established comprehensively considering the principle of mass and energy conservation and relevant heat balance theory, as shown in Fig. 3, and the involved assumptions are given by [26–28]:

- The system works in the steady state.
- The heat dissipation loss from the system to the environment is not considered.
- The pressure loss of various pumps is not considered.
- Membrane fouling and wetting in the VMD module are ignored.

3.1. VMD module

The VMD module is utilized to concentrate and separate the feed solution, and the involved mass and energy balance equations are expressed as follows:

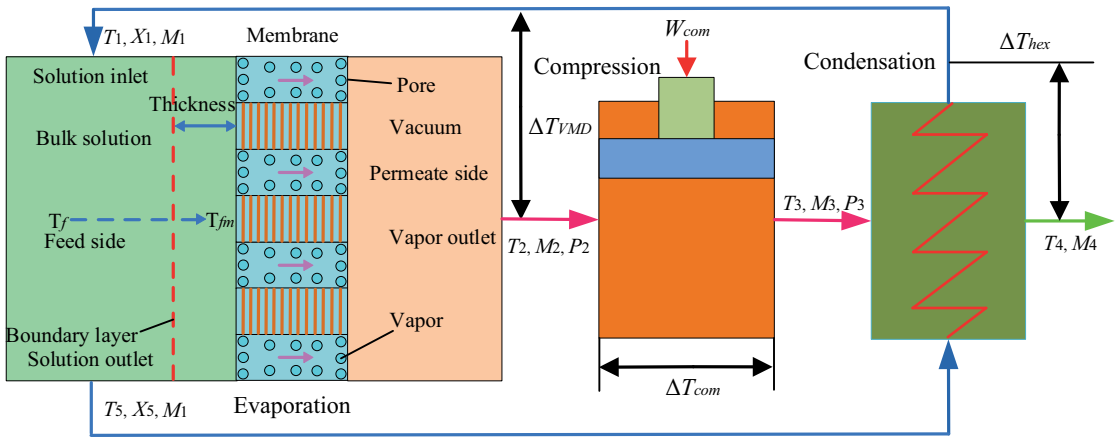

Fig. 3. Mass and energy balances within the current system.

$$M_1 = M_2 + M_5 \tag{1}$$

$$M_1 X_1 = M_5 X_5 \tag{2}$$

$$M_1 h_1 = M_2 h_2 + M_5 h_5 \tag{3}$$

where h_1, h_2 and h_5 are the specific enthalpies for the inlet solution, vapor and outlet solution, respectively. M_1, M_2 and M_5 are mass flow rates for inlet solution, vapor and outlet solution, respectively. X_1 and X_5 are the inlet and outlet solution concentrations, respectively.

The heat transfer process, from the bulk solution to the membrane surface across the boundary layer, is expressed as follows [29]:

$$Q_f = h_f \left(T_f - T_{\text{fm}}\right) \tag{4}$$

where Q_f is the transferred heat, T_f and T_{fm} represent the bulk solution and membrane surface temperatures.

The heat transfer coefficient, h_f, can be written as follows [30]:

$$h_f = \frac{y\lambda \text{Re}^l \text{Pr}^z}{d} \tag{5}$$

where l, y and z stand for characteristic constants. d stands for the hydraulic diameter. Re and Pr stand for the Reynolds number and Prandtl number, which can be given by:

$$\text{Re} = \frac{vd\rho}{\mu} \tag{6}$$

$$\text{Pr} = \frac{C_p \mu}{\lambda} \tag{7}$$

where v represents the flow velocity of the fluid.

The heat transfer (Q_m) across the membrane, without considering heat conduction, can be expressed as follows:

$$Q_m = N\Delta H \tag{8}$$

where N and ΔH are the membrane flux and evaporation enthalpy, respectively.

Accordingly, the heat transfer balance equation in the VMD process is expressed as follows:

$$h_f \left(T_f - T_{\text{fm}}\right) = N\Delta H \tag{9}$$

In addition, the expression of mass transfer across the boundary layer can be expressed as follows [24]:

$$\frac{K_f d}{D_L} = \text{Sh} = 0.664 \left(\text{Re}\right)^{\frac{1}{2}} \left(\text{Sc}\right)^{\frac{1}{3}} \tag{10}$$

$$\text{Sc} = \frac{\mu}{\rho D_L} \tag{11}$$

where K_f and D_L stand for the solute mass transfer coefficient through the boundary layer and the liquid phase's diffusion coefficient, respectively. Sh and Sc stand for the Sherwood and Schmidt numbers, respectively.

Furthermore, the expression of mass transfer across the membrane is written as follows [31]:

$$N = K_m \Delta P = \left[1.064 \frac{r\varepsilon}{\tau\delta}\left(\frac{M_m}{\text{RT}_m}\right)^{1/2} + 0.125 \frac{r^2\varepsilon}{\tau\delta}\left(\frac{M_m P_m}{\mu_v \text{RT}_m}\right)\right]\Delta P \tag{12}$$

The driving pressure difference across the membrane is written as follows [32]:

$$\begin{aligned}\Delta P &= P_{\text{sm}} - P_2 = \left(x_{\text{wm}}\left(1 - 0.5x_{\text{fm}} - 10x_{\text{fm}}^2\right)\right)P_{\text{fm}} - P_2 \\ &= \left(x_{\text{wm}}\left(1 - 0.5x_{\text{fm}} - 10x_{\text{fm}}^2\right)\right)\exp\left(23.238 - \frac{3841}{T_{\text{fm}} - 45}\right) - P_2\end{aligned} \tag{13}$$

where K_m is the mass transfer coefficient. M_m is the water molecular weight. R is the ideal gas constant. r, ε, δ and τ represent the pore size, porosity, thickness and tortuosity of membrane. T_m represents the average membrane pore temperature. P_m and ΔP represent the average membrane pore pressure and driving pressure difference, respectively.

x_{fm} and x_{wm} stand for the mole fractions for the sulfuric acid and water, respectively. P_{fm} represents the saturated vapor pressure of the water at T_{fm}.

3.2. Compressor

The compressor is employed to compress the secondary vapor, aiming to obtain higher saturated temperature and pressure. The compressor outlet temperature is expressed as follows [22]:

$$T_3 = T_2 \left(I\right)^{\frac{k-1}{k}} = T_2 \left(\frac{P_3}{P_2}\right)^{\frac{k-1}{k}} \tag{14}$$

where T_2 and T_3 represent the compressor inlet and outlet temperatures, respectively. P_2 and P_3 represent the compressor inlet and outlet pressures, respectively. k is the thermal insulation coefficient. I is the compression ratio.

The power consumption in the compression process is as follows [33]:

$$W_{\text{com}} = \frac{\left(h_3 - h_2\right)M_2}{\eta_{\text{th}} \cdot \eta_{\text{me}} \cdot \eta_{\text{mo}}} \tag{15}$$

where h_2 and h_3 stand for the inlet and outlet specific enthalpies, respectively. η_{me}, η_{mo} and η_{th} stand for the mechanical, motor and thermal efficiencies, respectively.

For the proposed system, the compressor power is determined by the saturated temperature difference between the inlet and outlet (ΔT_{com}), which can be expressed as follows:

$$\Delta T_{com} = \Delta T_{hex} + \left(T_1 - T_{sp}\right) = \Delta T_{hex} + \Delta T_{VMD} \tag{16}$$

where ΔT_{hex} stands for the heat transfer temperature difference within the heat exchanger. T_{sp} stands for the saturated temperature at P_2 ΔT_{VMD} stands for the temperature difference between inlet solution and outlet saturated vapor.

3.3. Heat exchanger

As a heat exchange unit, the heat exchanger is used to recover and reuse the vaporization heat, and the relevant energy balance equation is presented as follows:

$$M_5\left(h_6 - h_5\right) = M_3\left(h_3 - h_4\right) \tag{17}$$

where M_3 stands for the mass flow rate of the compressed vapor. h_4 and h_6 are the specific enthalpies of condensate and solution at the outlet, respectively.

The heat transfer area of heat exchanger is shown as follows:

$$A = \frac{M_3\left(h_3 - h_4\right)}{U\Delta t_{LMTD}} \tag{18}$$

where U stands for the heat transfer coefficient. ΔT_{LMTD} stands for the logarithmic heat transfer temperature difference, which can be expressed as follows:

$$\Delta t_{LMTD} = \frac{\left(T_3 - T_6\right) - \left(T_4 - T_5\right)}{\ln\left(\frac{T_3 - T_6}{T_4 - T_5}\right)} \tag{19}$$

3.4. Exergy

Exergy performance can reflect the irreversible energy loss within the thermodynamic system. In this section, exergy analysis is introduced to assess the coupled system. For the convenience of calculation and analysis, the reference state parameters, such as ambient temperature, ambient pressure and solution concentration, are assumed to be 298.15 K, 0.1 MPa and 5%, respectively. Generally, exergy mainly consists of the physical exergy and chemical exergy. For the current system, the working medium contains sulfuric acid solution, liquid water and vapor. Water and vapor have only physical exergy without considering the chemical exergy, which can be expressed as follows [34]:

$$e_p = \left(h - h_0\right) - T_0\left(s - s_0\right) \tag{20}$$

where e_p represents the specific physical exergy. T_0, h_0 and s_0 stand for the temperature, specific enthalpy and specific entropy at the ambient reference state, respectively. h and s stand for the specific enthalpy and specific entropy at the calculated state, respectively.

The treated sulfuric acid solution for the current system is considered to be mixed with sulfuric acid and pure water, its specific exergy, e, is given by [22]:

$$e = e_p + e_c \tag{21}$$

$$e_p = C_p\left(T - T_0 - T_0\ln\left(\frac{T}{T_0}\right)\right) \tag{22}$$

$$e_c = T_0\left(R_s X_s \ln\left(\frac{x_s}{x_{s0}}\right) + R_w X_w \ln\left(\frac{x_w}{x_{w0}}\right)\right) \tag{23}$$

where e_c stands for the specific chemical exergy. x_s and X_s stand for the molar fraction and mass fraction for the sulfuric acid at the calculated state, respectively. x_w and X_w stand for the molar fraction and mass fraction for the water at the calculated state, respectively. x_{s0} and x_{w0} stand for the molar fractions for the sulfuric acid and water at the reference state.

After obtaining the exergy values of each point within the system, the exergy destruction should be calculated to evaluate system exergy performance. The exergy destructions of the components within the system are presented as follows [35]:

$$E_{dVMD} = M_1 e_1 - M_5 e_5 - M_2 e_2 \tag{24}$$

$$E_{dhex} = M_2 e_3 + M_5 e_5 - M_2 e_4 - M_5 e_1 \tag{25}$$

$$E_{dcom} = \left(1 - \eta_{mo}\right) W_{com} + \left(1 - \eta_{com}\right)\eta_{mo} W_{com} \tag{26}$$

$$E_{dpum} = \left(1 - \eta_{mo}\right) W_{pum} + \frac{T_0}{T_{pum}}\left(1 - \eta_{pum}\right) W_{pum} \tag{27}$$

where E_{dVMD}, E_{dhex}, E_{dcom} and E_{dpum} represent the exergy destructions of the VMD module, heat exchanger, compressor and pump, respectively. e_1, e_2, e_3, e_4 and e_5 represent the specific exergies at points 1–5 within the system, respectively. η_{com} and η_{pum} represent the compressor efficiency and feed pump efficiency, respectively. T_{pum} represents the temperature of feed solution flowing through the feed pump, respectively. W_{pum} is the feed pump power, which can be expressed as follows:

$$W_{pum} = \frac{M_1 \rho g}{3.6 \times 10^6 \eta_{pum}}\left(\Delta Z + \frac{v^2}{2g}\right) \tag{28}$$

where g and ΔZ stand for the gravity acceleration and lift of pump, respectively.

Exergy efficiency is defined as the ratio of exergy output and exergy input for the current system. The exergy input includes the power of the compressor and feed pump, while the energy output includes the exergy of the condensate and concentrate solution. The exergy efficiency is expressed as follows [36]:

$$\eta_{exe} = \frac{E_{out}}{E_{in}} \times 100\% \quad (29)$$

On the basis of the above established mathematical models, the numerical simulation is carried out by solving the equilibrium equations iteratively with the aid of MATLAB software, and the detailed design parameters for simulation is presented in Table 1.

4. Results and discussion

4.1. Model validation

The mathematical models applied in the current system have been verified by the experimental data. The feed concentration, feed temperature and permeate side pressure were fixed at 2%, 353 K and 41 kPa both in the simulation and experiment work, Fig. 4 shows the comparison of experimental and simulated membrane flux with the feed velocity in the range of 1.0–1.5 m·s^{-1}, it was clear that the simulated curve of membrane flux was close to the experimental values under the same operation conditions, and the relative error was found to be within 20%. Obviously, there was some deviation between numerical simulation and experimental results, the main reason was that: (1) The influence of energy loss was not considered in the simulation process, which made the simulation results more ideal than the experiment; (2) In the experimental process, due to the limitation of the accuracy of the test equipment, there was a large error in the measurement of water production. However, the above comparison results indicated that the currently established models could ensure good accuracy and reliability in predicting experimental outcomes.

Table 1
Detailed design parameters for simulation

Parameters	Value
r (μm)	0.2
ε (%)	80
Membrane length (m)	0.8
Membrane area (m^2)	10–200
η_{th} (%)	76
η_{me} (%)	80
η_{mo} (%)	70

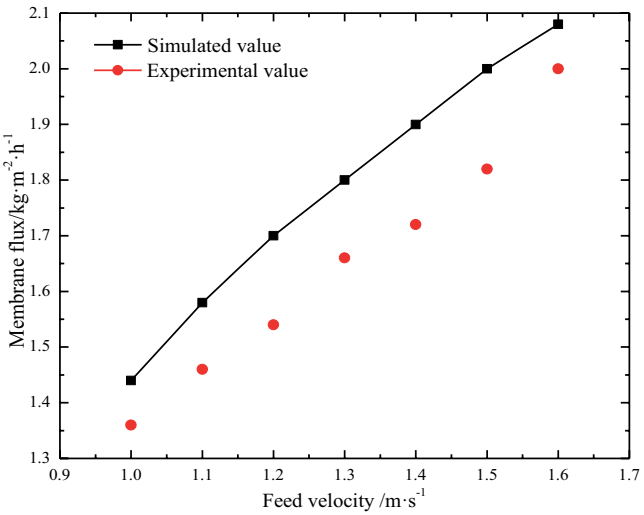

Fig. 4. Comparison of simulated and experimental results.

4.2. Analysis of mass and heat transfer characteristics

The system needs to preheat the feed solution to the set temperature through an external heat source when it starts. Then, under the action of the MVR process driven by electric power, the secondary vapor produced by the VMD process is compressed, then the compressed high-grade secondary vapor is used as a heating heat source to exchange heat with the treated feed solution in the heat exchanger, and finally condenses into the liquid. The whole process involves the heat and mass transfer. Therefore, the main content of this section is to study the influences of operation parameters such as feed concentration, feed temperature, feed velocity and permeate side pressure on the characteristics of heat and mass transfer process within the system.

Figs. 5 and 6 show the effects of feed concentration on the convective heat transfer coefficient and solute mass transfer coefficient when feed temperature, feed velocity and permeate side pressure are set to 358.15 K, 1.0 m·s^{-1} and 35 kPa, respectively. It can be seen that as the feed concentration increases from 5% to 35%, the convective heat transfer coefficient decreases and the solute mass transfer coefficient increases. This is because when the feed

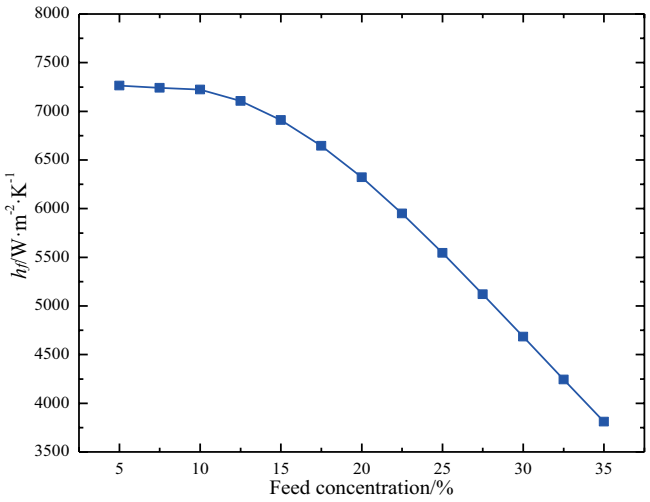

Fig. 5. Variation of heat transfer coefficient with feed concentration.

concentration increases, the viscosity of the main solution increases, the activity of water molecule decreases, and the activity of sulfuric acid molecule increases, then a large number of sulfuric acid molecules migrate from the bulk solution to the membrane surface, resulting in the increase of boundary layer thickness and boundary layer resistance. Therefore, the heat and mass transfer process of water molecule from the bulk solution through the thermal boundary layer to the membrane surface decreases, and the relevant convective heat transfer coefficient decreases. Since the concentration of solute molecules on the membrane surface is high, the mass transfer coefficient of sulfuric acid molecule is considered to be elevated. Obviously, the elevation of feed concentration is helpful to promote the transport of solute molecule rather than water molecule, which will degrades the performance of the coupled process.

Figs. 7 and 8 show the effects of feed temperature on the convective heat transfer coefficient and mass transfer coefficient under different feed concentrations when the feed velocity and permeate side pressure are set to 1.0 m·s^{-1} and 35 kPa, respectively. It can be seen that when the feed concentration remains unchanged, with the increase of feed temperature from 353.15 to 363.15 K, the viscosity of the solution on the hot side decreases, the activities both of water molecules and sulfuric acid molecules in the solution increase, which strengthens the heat and mass transfer process, resulting in the increase of convective heat transfer coefficient and solute mass transfer coefficient from the bulk solution to the membrane surface across the boundary layer. Thus, a higher feed temperature can lead to the transport of the water molecule, which is benefical to improve the performance of the coupled process.

Figs. 9 and 10 show the effects of feed velocity on the convective heat transfer coefficient and mass transfer coefficient under different feed concentrations when the feed temperature and permeate side pressure are set to 358.15 K

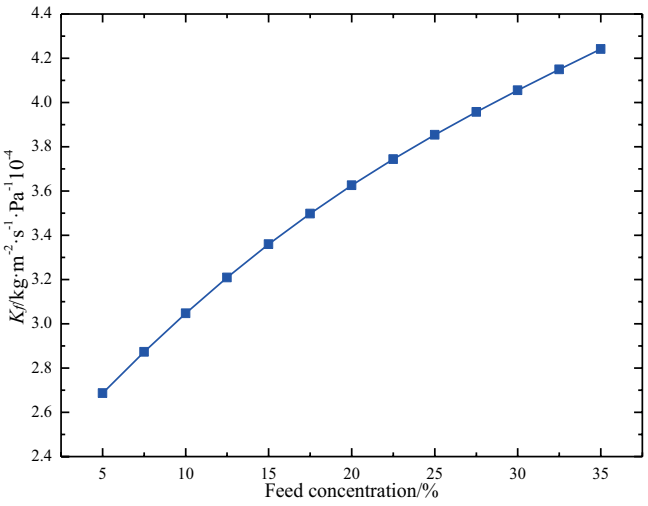

Fig. 6. Variation of mass transfer coefficient with feed concentration.

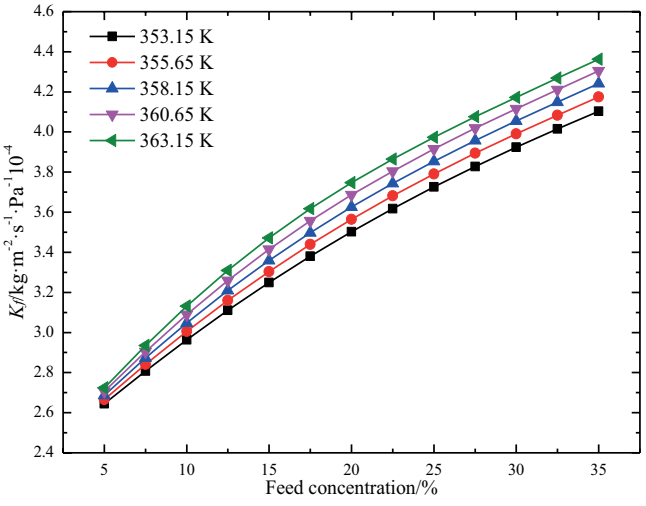

Fig. 8. Variation of mass transfer coefficient with feed concentration and feed temperature.

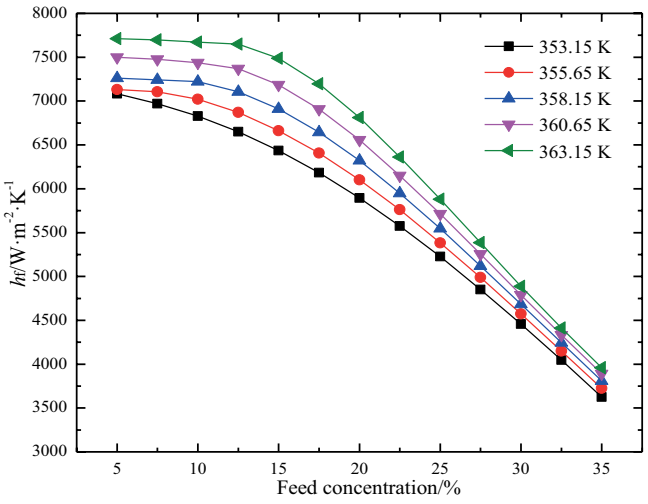

Fig. 7. Variation of heat transfer coefficient with feed concentration and feed temperature.

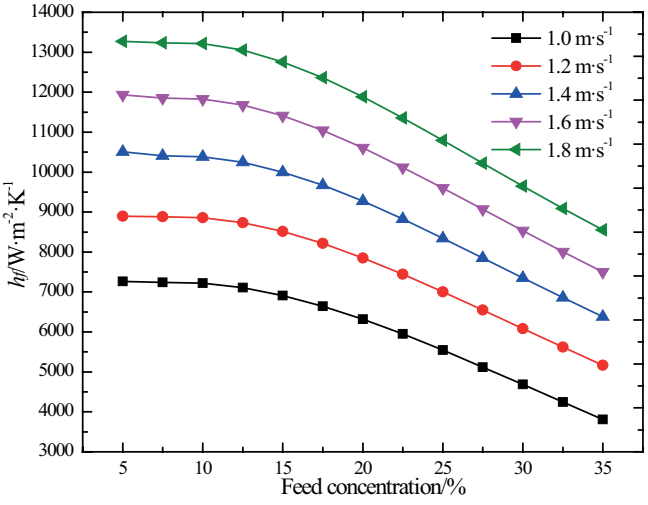

Fig. 9. Variation of heat transfer coefficient with feed concentration and feed velocity.

and 35 kPa, respectively. It can be seen that when the feed concentration remains unchanged, with the increase of the feed velocity from 1.0–1.8 m·s^{-1}, the flow state of the liquid in the VMD module is significantly changed, the fluid turbulence intensity increases, the solution Reynolds number increases, the thickness of the flow boundary layer decreases, the boundary layer resistance decreases, and the heat and mass transfer process is accelerated, resulting in the increase of convective heat transfer coefficient and mass transfer coefficient from the bulk solution to the membrane surface across the boundary layer. Apparently, a higher feed velocity contributes to the transport both of water and solute molecules, which can also help to enhance the performance of the coupled process.

Figs. 11 and 12 show the effects of permeate side pressure on the convective heat transfer coefficient and mass transfer coefficient under different feed concentrations when the feed temperature and feed velocity are set to 358.15 K and 1.0 m·s^{-1} respectively. It can be seen that when the feed concentration remains unchanged and permeate side pressure increases from 35 to 45 kPa, both of the convective heat transfer coefficient and mass transfer coefficient increase slightly. This is due to the fact that increasing the permeate side pressure directly leads to the reduction of the transmembrane driving pressure difference, which reduces the evaporation rate of water molecules on the surface of the hot side membrane to a certain extent, so as to reduce the vaporization heat of water molecules provided by the bulk solution. As a result, the temperature of bulk solution in the VMD module increases slightly, which leads to increase both of the convective heat transfer coefficient and solute mass transfer coefficient slightly from the bulk solution to the membrane surface across the boundary layer. Therefore, a higher permeate side pressure is not conducive to the evaporation and transport of water molecule in the VMD process.

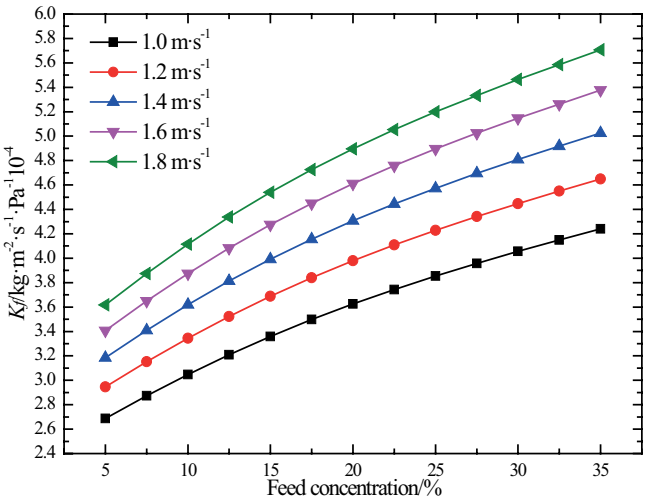

Fig. 10. Variation of mass transfer coefficient with feed concentration and feed velocity.

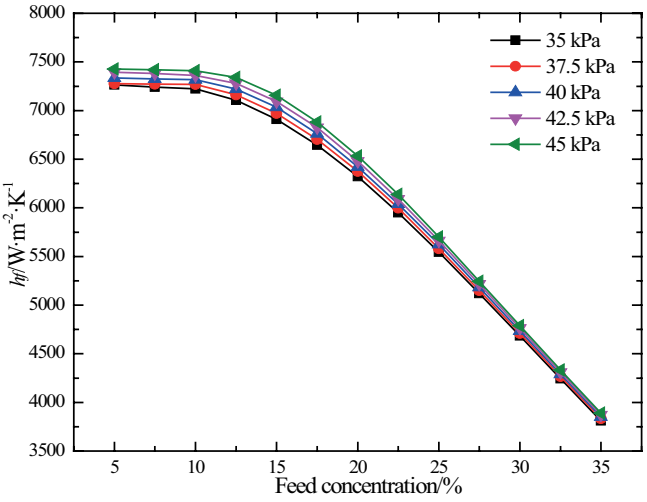

Fig. 11. Variation of heat transfer coefficient with feed concentration and permeate side pressure.

4.3. Analysis of energy efficiency

For the current system, the membrane area of the VMD module is an important parameter, which affects the evaporation capacity, energy consumption and evaporation cost of the system. Therefore, this section focuses on the influence mechanism of membrane area on system energy efficiency.

A parametric analysis is carried out as feed concentration, feed temperature and feed velocity are set to 5%, 358.15 K and 1.0 m·s^{-1}, respectively. Figs. 13–17 show the effects of membrane area on system performance including each point temperature, membrane flux, transfer area of heat exchanger, energy consumption, exergy efficiency and so on. In order to ensure uniform and stable water production, the evaporate rate is fixed at a constant value of 200 kg·h^{-1}. With the increase of membrane area from 10 m^2 to 200 m^2, the permeate side pressure increases from 37.35 to 55.98 kPa while membrane flux decreases from 20–1 kg·m^{-2}·h^{-1}. Here, the evaporation rate is firstly

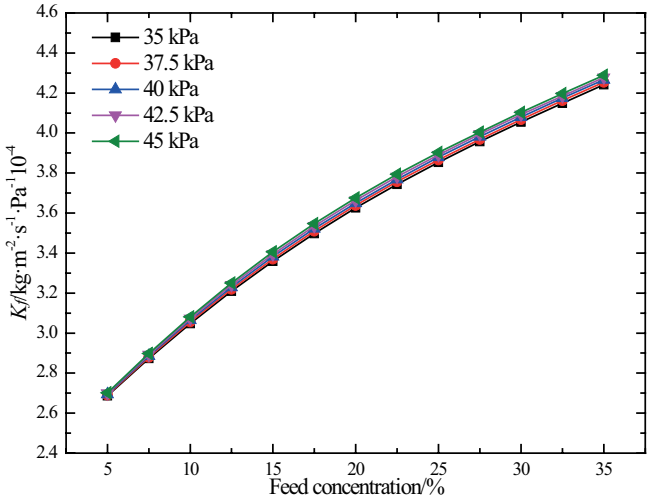

Fig. 12. Variation of mass transfer coefficient with feed concentration and permeate side pressure.

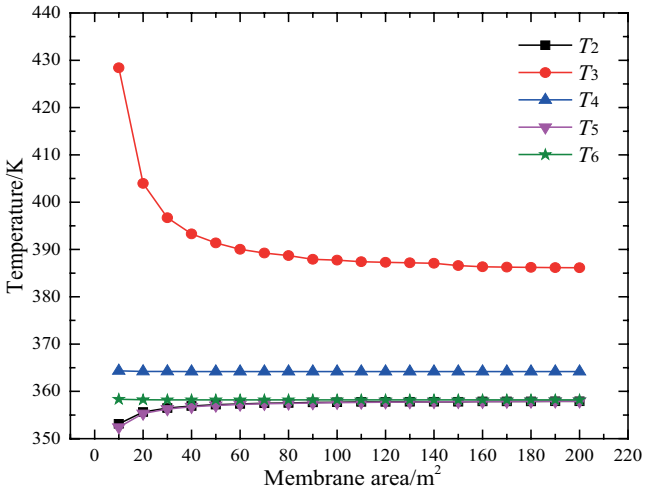

Fig. 13. Variation of each point temperature with membrane area.

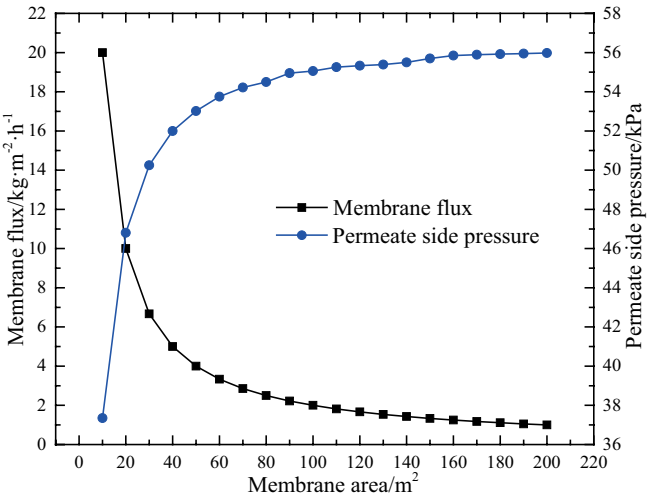

Fig. 14. Variation of membrane flux and permeate side pressure with membrane area.

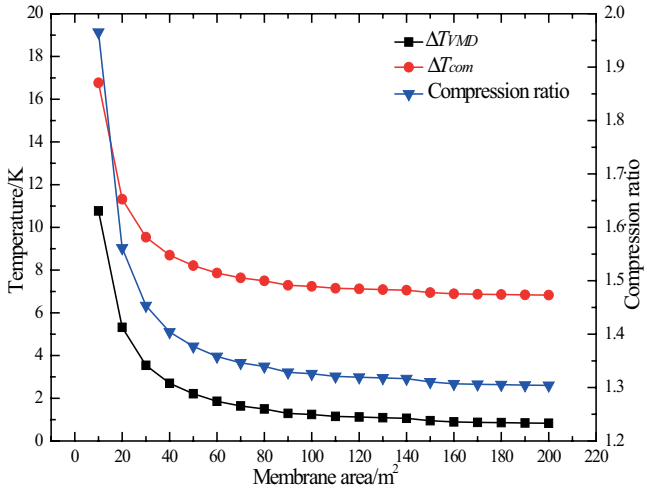

Fig. 15. Variation of ΔT_{VMD}, ΔT_{com} and compression ratio with membrane area.

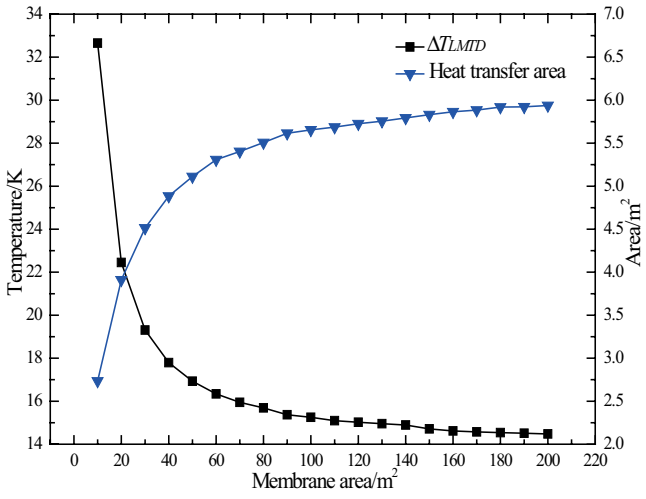

Fig. 16. Variation of ΔT_{LMTD} and heat transfer area with membrane area.

defined as the product of membrane flux and membrane area. As the evaporation rate is kept constant, the membrane flux must decrease with the increase of membrane area. Therefore, the permeate side pressure can only be increased when the feed concentration, feed temperature and feed flow rate remain unchanged. Thus, the temperature of secondary vapor (T_2) is observed to be increased from 353.14–357.89 K. It should be pointed out that the pressure at the compressor outlet is fixed at 73 kPa in the simulation process, due to the increase of pressure at the compressor inlet, the compression ratio reduces from 1.97 to 1.30, resulting in the decrease of the temperature at the compressor outlet from 428.42–386.13 K, while the corresponding condensation temperature of secondary vapor (T_4) is maintain as 364.15 K. Thus, a significant drop of ΔT_{VMD} for the VMD module and ΔT_{com} for the compressor can be observed. However, for the aspect of concentrated solution of the VMD module, the temperature at the heat exchanger inlet increases from 352.41 to 357.91 K while the temperature at the heat exchanger outlet is always kept constant. In addition, it is also found that with the increase of membrane area from 10 to 200 m², the ΔT_{LMTD} of heat exchanger drops from 32.65 to 14.48 K while the heat transfer area of heat exchanger rises from 2.73 to 5.90 m². In addition, a higher membrane area requires higher feed flow rate, which increases the energy consumption of the feed pump. For the aspect of compressor power, feed pump power, total power as well as exergy efficiency, larger membrane area corresponds to a lower compressor power, but requires a higher feed pump power. Obviously, the total power consumption exhibits a decline first followed by a rise and the exergy efficiency shows a first rise followed by a decline with the increase in membrane area. Therefore, there is an optimal membrane area of 60 m² that minimizes the total power to 10.04 kW and maximizes the exergy efficiency to 19.06%.

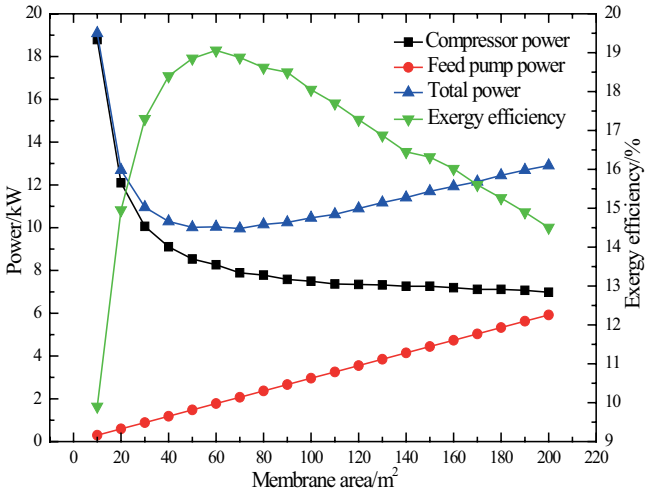

Fig. 17. Variation of compressor power, pump power, total power and exergy efficiency with membrane area.

5. Conclusions

This paper focused on employing a VMD system driven by a compressor to deal with sulfuric acid waste. Based on the established mathematical models, the influences from the operating parameters, such as feed concentration, feed temperature, feed velocity and permeate side pressure on the heat and mass transfer characteristics of the system were investigated. Furthermore, the effects of membrane area on system energy efficiency were also studied. The obtained significant findings after detailed simulation investigation were drawn as follows:

- It was concluded that increasing the feed concentration decreased the heat transfer coefficient, while increased the mass transfer coefficient, which strengthened the heat and mass transfer for the water molecules from the bulk solution to the membrane surface across the boundary layer. In addition, increasing the feed temperature, feed velocity and permeate side pressure led to the increase of the heat and mass transfer coefficients, resulting in the improvement of heat and mass transfer for the water molecules from the bulk solution to the membrane surface across the boundary layer.
- As feed concentration, feed temperature and feed velocity were set to 5%, 358.15 K and 1.0 m·s^{-1}, larger membrane area of the VMD module led to the higher permeate side pressure and lower membrane flux to ensure uniform and stable water production at the conditions of evaporate rate of 200 kg·h^{-1}. In addition, increasing membrane area decreased the values of ΔT_{VMD}, ΔT_{com}, ΔT_{LMTD} and compression ratio, but increased the heat transfer area of heat exchanger.
- Increasing membrane area decreased the compressor power and increased the feed pump power, which caused the total power consumption to exhibit a decline first followed by a rise and the exergy efficiency to exhibit a first rise followed by a decline. Therefore, there was an optimal membrane area of 60 m^2 that minimized the total power to 10.04 kW and maximized the exergy efficiency to 19.06%.
- The above obtained results prove that the application of the current system in the sulfuric acid waste treatment is an interesting approach. The present study mainly focuses on the evaporation characteristics of system based on the simulation research. Consequently, more experiments under multiple working conditions will be performed in the future, which will provide significant references and technical support for the optimization and commercial application of the current system.

Acknowledgments

The authors acknowledge the financial support from the National Natural Science Foundation of China (No. 52105387), China Postdoctoral Science Foundation (No. 2021M692349), Natural Science Research Projects of General Universities in Jiangsu Province (No. 21KJB460019), Hong Kong Scholars Program (No. XJ2021032).

Symbols

A	—	Area, m^2
C_p	—	Heat capacity, kJ·kg^{-1}·K^{-1}
d	—	Hydraulic diameter at the feed bulk solution, m
e	—	Specific exergy, kJ·kg^{-1}
E	—	Exergy, kW
h	—	Specific enthalpy, kJ·kg^{-1}
h_f	—	Heat transfer coefficient through the thermal boundary layer, W·m^{-2}·K^{-1}
I	—	Compression ratio
k	—	Thermal insulation coefficient
K_f	—	Solute mass transfer coefficient, kg·m^{-2}·s^{-1}·Pa^{-1}
K_m	—	Mass transfer coefficient across the membrane, kg·m^{-2}·s^{-1}·Pa^{-1}
l	—	Characteristic constant
M	—	Mass flow rate, kg·s^{-1}
M_m	—	Molecular weight of water
N	—	Membrane flux, kg·m^{-2}·h^{-1}
Nu	—	Nusselt number
P	—	Pressure, kPa
Pr	—	Prandtl number
Q_f	—	Heat flux through the thermal boundary layer, W·m^{-2}
Q_m	—	Heat flux across the membrane, W·m^{-2}
r	—	Membrane pore size, μm
R	—	Ideal gas constant, J·mol^{-1}·°C^{-1}
Re	—	Reynolds number
T	—	Thermodynamic temperature, K
U	—	Heat transfer coefficient, W·m^{-2}·K^{-1}
v	—	Flow velocity, m·s^{-1}
W	—	Power, W
X	—	Mass concentration
x	—	Mole fraction
y	—	Characteristic constant
z	—	Characteristic constant
ΔH	—	Enthalpy of evaporation for water molecule, kJ·kg^{-1}

Abbreviations

AGMD	—	Air gap membrane distillation
DCMD	—	Direct contact membrane distillation

SGMD — Sweeping gas membrane distillation
SHEC — Specific heating energy consumption
VMD — Vacuum membrane distillation

Greek

δ — Thickness, m
ε — Porosity
η — Efficiency
λ — Thermal conductivity, $W \cdot m^{-1} \cdot °C^{-1}$
μ — Dynamic viscosity, Pa·s
ρ — Density, $kg \cdot m^{-3}$
τ — Tortuosity

Subscripts

c — Chemical
com — Compressor
d_{com} — Destruction of compressor
d_{hex} — Destruction of heat exchanger
d_{pum} — Destruction of pump
d_{VMD} — Destruction of VMD module
exe — Exergy
f — Feed side
fm — Membrane surface in feed side
hex — Heat exchanger
in — Input
m — Membrane
me — Mechanical
mo — Motor
out — Output
p — Physical
pum — Pump
s — Sulfuric acid
sm — Saturated state at the membrane surface
sp — Saturated state in permeate side
th — Thermal
VMD — Vacuum membrane distillation
w — Water
wm — Water molecule in the solution of membrane surface

References

[1] H. Liu, J. Xia, K. Cui, J. Meng, R. Zhang, B. Cao, P. Li, Fabrication of high-performance pervaporation membrane for sulfuric acid recovery via interfacial polymerization, J. Membr. Sci., 624 (2021) 119108, doi: 10.1016/J.MEMSCI.2021.119108.
[2] H. Guo, P. Yuan, V. Pavlovic, J. Barber, Y. Kim, Ammonium sulfate production from wastewater and low-grade sulfuric acid using bipolar- and cation-exchange membranes, J. Cleaner Prod., 285 (2021) 124888, doi: 10.1016/J.JCLEPRO.2020.124888.
[3] T. Ouyang, J. Xu, Z. Su, Z. Zhao, G. Huang, C. Mo, A novel design of low-grade waste heat utilization for coal-fired power plants with sulfuric acid recovery, Energy Convers. Manage., 227 (2021) 113640, doi: 10.1016/j.enconman.2020.113640.
[4] A. Bamasag, H. Daghooghi-Mobarakeh, T. Alqahtani, P. Phelan, Performance enhancement of a submerged vacuum membrane distillation (S-VMD) system using low-power ultrasound, J. Membr. Sci., 621 (2021) 119004, doi: 10.1016/j.memsci.2020.119004.
[5] G. Viader, O. Casal, B. Lefèvre, N. de Arespacochaga, C. Echevarría, J. López, C. Valderrama, J.L. Cortina, Integration of membrane distillation as volume reduction technology for in-land desalination brines management: pre-treatments and scaling limitations, J. Environ. Manage., 289 (2021) 112549, doi: 10.1016/ J.JENVMAN.2021.112549.
[6] P. Boutikos, E.Sh. Mohamed, E. Mathioulakis, V. Belessiotis, A theoretical approach of a vacuum multi-effect membrane distillation system, Desalination, 422 (2017) 25–41.
[7] E.S. Mohamed, P. Boutikos, E. Mathioulakis, V. Belessiotis, Experimental evaluation of the performance and energy efficiency of a vacuum multi-effect membrane distillation system, Desalination, 408 (2017) 70–80.
[8] J.-P. Mericq, S. Laborie, C. Cabassud, Evaluation of systems coupling vacuum membrane distillation and solar energy for seawater desalination, Chem. Eng. J., 166 (2011) 596–606.
[9] H. Dahmardeh, H.A. Akhlaghi Amiri, S.M. Nowee, Evaluation of mechanical vapor recompression crystallization process for treatment of high salinity wastewater, Chem. Eng. Process., 145 (2019) 107682, doi: 10.1016/ j.cep.2019.107682.
[10] Y. Kansha, A. Kishimoto, A. Tsutsumi, Application of the self-heat recuperation technology to crude oil distillation, Appl. Therm. Eng., 43 (2012) 153–157.
[11] S. Ai, B. Wang, X. Li, W. Shi, Numerical analysis on the performance of mechanical vapor recompression system for strong sodium chloride solution enrichment, Appl. Therm. Eng., 137 (2018) 386–394.
[12] L. Liang, D. Han, R. Ma, Treatment of high-concentration wastewater using double-effect mechanical vapor recompression, Desalination, 314 (2013) 139–146.
[13] J. Yang, C. Zhang, Z. Zhang, L. Yang, Electroplating wastewater concentration system utilizing mechanical vapor recompression, J. Environ. Eng., 144 (2018) 04018053, doi: 10.1061/(ASCE)EE.1943-7870.0001380.
[14] D. Han, J. Chen, T. Zhou, Experimental investigation of a batched mechanical vapor recompression evaporation system, Appl. Therm. Eng., 192 (2021) 116940, doi: 10.1016/j.applthermaleng.2021.116940.
[15] Y. Zhou, C. Shi, G. Dong, Analysis of a mechanical vapor recompression wastewater distillation system, Desalination, 353 (2014) 91–97.
[16] A.S. Nafey, H.E.S. Fath, A.A. Mabrouk, Thermoeconomic design of a multi-effect evaporation mechanical vapor compression (MEE–MVC) desalination process, Desalination, 230 (2008) 1–15.
[17] Y. Zhang, Y. Peng, S. Ji, Z. Li, P. Chen, Review of thermal efficiency and heat recycling in membrane distillation processes, Desalination, 367 (2015) 223–239.
[18] J.A. Leon, R. Palacios-Bereche, S.A. Nebra, Batch pervaporative fermentation with coupled mebrane and its influence on energy consumption in permeate recovery and distillation stage, Energy, 109 (2016) 77–91.
[19] Y. Wang, B. Qiu, Z. Xiao, J. Liu, S. Fan, Hybrid desalination system of mechanical vapor recompression based on membrane distillation, Membr. Water Treat., 12 (2021) 115–123.
[20] J. Li, W. Zhou, S. Fan, Z. Xiao, Y. Liu, J. Liu, B. Qiu, Y. Wang, Bioethanol production in vacuum membrane distillation bioreactor by permeate fractional condensation and mechanical vapor compression with polytetrafluoroethylene (PTFE) membrane, Bioresour. Technol., 268 (2018) 708–714.
[21] Z. Si, D. Han, Y. Song, J. Chen, L. Luo, R. Li, Experimental investigation on a combined system of vacuum membrane distillation and mechanical vapor recompression, Chem. Eng. Process., 139 (2019) 172–182.
[22] Z. Si, D. Han, J. Gu, Y. Song, Exergy analysis of a vacuum membrane distillation system integrated with mechanical vapor recompression for sulfuric acid waste treatment, Appl. Therm. Eng., 178 (2020) 115516, doi: 10.1016/j.applthermaleng.2020.115516.
[23] Z. Si, D. Han, J. Xiang, Experimental investigation on the mechanical vapor recompression evaporation system coupled with multiple vacuum membrane distillation modules to treat industrial wastewater, Sep. Purif. Technol., 275 (2021) 119178, doi: 10.1016/j.seppur.2021.119178.
[24] Z. Si, D. Han, J. Gu, Y. Song, P. Zhang, Characteristics analysis of a combined system of vacuum membrane distillation

and mechanical vapor recompression, Desal. Water Treat., 171 (2019) 29–43.
[25] Z. Si, D. Han, Y. Xing, J. Xiang, Experimental and numerical study on thermodynamic characteristics of a vacuum membrane distillation system based on mechanical vapor recompression for sulfuric acid waste, Chem. Eng. Process., 174 (2022) 108862, doi: 10.1016/j.cep.2022.108862.
[26] V. Karanikola, S.E. Moore, A. Deshmukh, Economic performance of membrane distillation configurations in optimal solar thermal desalination systems, Desalination, 472 (2019) 114164, doi: 10.1016/j.desal.2019.114164.
[27] M.M.A. Shirazi, A. Kargari, M. Tabatabaei, Evaluation of commercial PTFE membranes in desalination by direct contact membrane distillation, Chem. Eng. Process., 76 (2014) 16–25.
[28] U.K. Kesieme, N. Milne, C.Y. Cheng, Recovery of water and acid from leach solutions using direct contact membrane distillation, Water. Sci. Technol., 69 (2013) 868–875.
[29] X. Li, Y. Qin, R. Liu, Study on concentration of aqueous sulfuric acid solution by multiple-effect membrane distillation, Desalination, 307 (2012) 34–41.
[30] J.I. Mengual, M. Khayet, M.P. Godino, Heat and mass transfer in vacuum membrane distillation, Int. J. Heat Mass Transfer, 47 (2004) 865–875.
[31] R.H. Liu, D. Chen, Y.L. Peng, Mathematical modeling and optimal operation condition analysis of heat pump two-effect direct contact membrane distillation system, Mater. Sci. Eng., 612 (2019) 032004, doi: 10.1088/1757-899X/612/3/032004.
[32] S.Gh. Lovineh, M. Asghari, B. Rajaei, Numerical simulation and theoretical study on simultaneous effects of operating parameters in vacuum membrane distillation, Desalination, 314 (2013) 59–66.
[33] W.K. Pang, W.J. Ling, Q.L. Pan, Performance analysis of mechanical vapor recompression heat pump driven by centrifuge fan, J. Mech. Eng., 49 (2013) 142–146 (in Chinese).
[34] R. Miladi, N. Frikha, S. Gabsi, Exergy analysis of a solar-powered vacuum membrane distillation unit using two models, Energy, 120 (2017) 872–883.
[35] D. Han, W.F. He, C. Yue, W.H. Pu, Study on desalination of zero-emission system based on mechanical vapor compression, Appl. Energy, 185 (2017) 1490–1496.
[36] J. Lin, G. Qin, C. Jia, Design and experimental analysis of a vapor compression heat pump combined with double-stage forced-circulation evaporators, Energy Sci. Eng., 6 (2018) 523–534.